The Astrophysical Journal, 993:94 (12pp), 2025 November 1 https://doi.org/10.3847/1538-4357/ae0645
© 2025. The Author(s). Published by the American Astronomical Society.
OPEN ACCESS

Two Decades of Dust Evolution in SN 2005af through JWST, Spitzer, and Chemical Modeling

Arkaprabha Sarangi[1,2], Szanna Zsíros[3], Tamás Szalai[3,4], Laureano Martinez[5], Melissa Shahbandeh[6], Ori D. Fox[6], Schuyler D. Van Dyk[7], Alexei V. Filippenko[8], Melina Cecilia Bersten[5,9,10], Ilse De Looze[11], Chris Ashall[12], Tea Temim[13], Jacob E. Jencson[14], Armin Rest[15,16], Dan Milisavljevic[17], Luc Dessart[18], Eli Dwek[19], Nathan Smith[20], Samaporn Tinyanont[21], Thomas G. Brink[8], WeiKang Zheng[8], Geoffrey C. Clayton[22], and Jennifer Andrews[23]

[1] Indian Institute of Astrophysics, 100 Feet Rd, Koramangala, Bengaluru, Karnataka 560034, India; arkaprabha.sarangi@iiap.res.in
[2] DARK, Niels Bohr Institute, University of Copenhagen, Jagtvej 155A, 2200 Copenhagen, Denmark
[3] Department of Experimental Physics, Institute of Physics, University of Szeged, Dóm tér 9, 6720 Szeged, Hungary
[4] MTA-ELTE Lendület "Momentum" Milky Way Research Group, Hungary
[5] Instituto de Astrofísica de La Plata (IALP), CCT-CONICET-UNLP, Paseo del Bosque S/N, B1900FWA, La Plata, Argentina
[6] Space Telescope Science Institute, 3700 San Martin Drive, Baltimore, MD 21218, USA
[7] Caltech/IPAC, Mailcode 100-22, Pasadena, CA 91125, USA
[8] Department of Astronomy, University of California, Berkeley, CA 94720-3411, USA
[9] Facultad de Ciencias Astronómicas y Geofísicas Universidad Nacional de La Plata, Paseo del Bosque S/N B1900FWA, La Plata, Argentina
[10] Kavli IPMU (WPI), UTIAS, The University of Tokyo, Kashiwa, Chiba 277-8583, Japan
[11] Sterrenkundig Observatorium, Ghent University, Krijgslaan 281 - S9, 9000 Gent, Belgium
[12] Institute for Astronomy, University of Hawai'i at Manoa, 2680 Woodlawn Dr., Honolulu, HI 96822, USA
[13] Department of Astrophysical Sciences, Princeton University, 4 Ivy Lane, Princeton, NJ 08544, USA
[14] IPAC, California Institute of Technology, 1200 E. California Blvd., Pasadena, CA 91125, USA
[15] Space Telescope Science Institute, Baltimore, MD 21218, USA
[16] Department of Physics and Astronomy, The Johns Hopkins University, Baltimore, MD 21218, USA
[17] Purdue University, Department of Physics and Astronomy, 525 Northwestern Ave, West Lafayette, IN 47907, USA
[18] Institut d'Astrophysique de Paris, CNRS-Sorbonne Université, 98 bis boulevard Arago, F-75014 Paris, France
[19] Observational Cosmology Lab, NASA Goddard Space Flight Center, Mail Code 665, Greenbelt, MD 20771, USA
[20] Steward Observatory, University of Arizona, 933 N. Cherry St, Tucson, AZ 85721, USA
[21] National Astronomical Research Institute of Thailand, 260 Moo 4, Donkaew, Maerim, Chiang Mai, 50180, Thailand
[22] Department of Physics & Astronomy, Louisiana State University, Baton Rouge, LA 70803, USA
[23] Gemini Observatory, 670 N. Aohoku Place, Hilo, HI 96720, USA
Received 2025 April 28; revised 2025 September 9; accepted 2025 September 10; published 2025 October 28

Abstract

The evolution of dust in core-collapse supernovae (SNe), in general, is poorly constrained owing to a lack of infrared observations a few years after explosion. Most theories of dust formation in SNe heavily rely only on SN 1987A. In the last two years, the James Webb Space Telescope (JWST) has enabled us to probe the dust evolution in decades-old SNe, such as SN 2004et, SN 2005ip, and SN 1980K. In this paper, we present two decades of dust evolution in SN 2005af, combining early-time infrared observations with the Spitzer Space Telescope and recent detections by the JWST. We have used a chemical kinetic model of dust synthesis in SN ejecta to develop a template of dust evolution in SN 2005af. Moreover, using this approach, for the first time, we have separately quantified the dust formed in the pre-explosion wind that survived after the explosion and the dust formed in the metal-rich SN ejecta post-explosion. We report that in SN 2005af, predominantly carbon-rich dust formed in the ejecta, with a total mass of at least 0.02 $M_{\odot}$. In the circumstellar medium, the surviving oxygen-rich dust amounts to about (3–6) $\times 10^{-3}$ $M_{\odot}$, yielding a total dust mass of at least 0.025 $M_{\odot}$.

Unified Astronomy Thesaurus concepts: Dust formation (2269); Core-collapse supernovae (304); James Webb Space Telescope (2291); Circumstellar dust (236); Infrared photometry (792)

1. Introduction

Core-collapse supernovae (SNe) are considered to be significant dust producers in galaxies (P. Bouchet & I. J. Danziger 1993; D. H. Wooden et al. 1993; E. Dwek 2006; C. Gall et al. 2011; T. Szalai & J. Vinkó 2013; M. Matsuura 2017; A. Sarangi et al. 2018b; T. Szalai et al. 2019). Dust produced in various SNe may vary in total mass, composition, and formation timescale. Infrared (IR) observations of several SNe in their first few years post-explosion have confirmed the presence of dust in their environment (e.g., R. Kotak et al. 2006; B. E. K. Sugerman et al. 2006; J. E. Andrews et al. 2010; W. P. S. Meikle et al. 2011; T. Szalai & J. Vinkó 2013; T. Szalai et al. 2019). With the arrival of the James Webb Space Telescope (JWST), mid-infrared (mid-IR) observations uncovered cold dust reservoirs in several historic SNe such as SN 2004et, SN 1980K, SN 1993J, SN 2005ip, and SN 2017eaw (M. Shahbandeh et al. 2023; S. Zsíros et al. 2024; M. Shahbandeh et al. 2025; T. Szalai et al. 2025).

The mass of dust inferred in an SN may vary from 10^{-4} $M_{\odot}$ to as large as 1 $M_{\odot}$ (C. Gall et al. 2014; M. Matsuura 2017; T. Szalai et al. 2019; F. D. Priestley et al. 2020; M. Niculescu-Duvaz et al. 2021; R. Wesson & A. Bevan 2021). This variation is often correlated with the epoch of measurement

Original content from this work may be used under the terms of the Creative Commons Attribution 4.0 licence. Any further distribution of this work must maintain attribution to the author(s) and the title of the work, journal citation and DOI.

and, to some extent, the instrument used for the detection. A moderate rate of dust formation is proposed to continue for several decades (R. Wesson et al. 2015; R. Wesson & A. Bevan 2021), gradually building up the dust mass over that period. Alternatively, the effect of large optical depths in SN ejecta at early times is also proposed as a reason behind the variance of dust masses (E. Dwek et al. 2019; A. Sarangi 2022) at various epochs of detection. Before the advent of JWST, there were hardly any SNe other than SN 1987A, which was bright enough for any mid-IR instrument after three or four years post-explosion. The dust formation sequence remained uncertain due to the lack of late-time measurements. Our JWST Cycle 1 programs GO-2666 and GO-1860 (PI O. Fox) have achieved phenomenal success in detecting several SNe, which are already a few decades old. This enables us to account for the dust masses in a population of nearby SNe, deriving a trend on dust formation in SNe in general.

Dust that is detected in an SN could be formed prior to the explosion, in the mass-loss winds (T. Verhoelst et al. 2009; I. Cherchneff 2013; T. Nozawa et al. 2014). Alternatively, it can form post-explosion, in the metal-rich ejecta and/or in a region of interaction between the SN shock wave and the circumstellar medium (CSM). Given the large distances of most SNe, observations do not have enough spatial resolution to locate where the dust is present or formed. Only nearby SN 1987A in LMC is an exception in this case, where the mass and location of dust have been traced over the last 35 yr (P. Bouchet & I. J. Danziger 1993; M. Matsuura et al. 2011; E. Dwek & R. G. Arendt 2015; M. Matsuura et al. 2015; R. G. Arendt et al. 2020; O. C. Jones et al. 2023). Overall, for SNe in general, the observed IR spectra do not provide a strong constraint on the location or timescale of dust formation. In this context, the uncertainties for the estimated dust masses, the chemical type of dust, and the timescale for dust formation remain unresolved.

In this paper, we assemble the data obtained for SN 2005af at optical, near-IR, and mid-IR wavelengths, using archival data of the Carnegie Supernova Project (CSP-I, optical photometry and spectrophotometry; M. Hamuy et al. 2006; J. P. Anderson et al. 2024), the Spitzer Space Telescope (hereafter Spitzer), and the newly obtained photometric data from JWST. We have conducted a complete study of dust evolution over two decades, owing to our successful imaging of SN 2005af ∼19 yr post-explosion, through our JWST GO-2666 program.

SN 2005af in NGC 4945, discovered in February 2005, is one of the closest known extragalactic SNe. The distance of the galaxy is debated to be either 3.47 ± 0.12 Mpc (B. A. Jacobs et al. 2009; G. S. Anand et al. 2021) or 3.9 Mpc (A. V. Filippenko & R. J. Foley 2005; C. Jacques & E. Pimentel 2005; R. Kotak et al. 2006). The SN was classified as a Type II-P core-collapse SN whose light curve was powered by radioactivity, with negligible evidence of interaction with any CSM (C. P. Gutiérrez et al. 2017; J. P. Anderson et al. 2024). The epoch of explosion has some uncertainty between MJD 53320.8 (C. P. Gutiérrez et al. 2017) and 53379 (T. Szalai & J. Vinkó 2013). We have chosen to use MJD 53320.8 based on more recent analysis of the SN light curve. Therefore, the epochs previously noted by T. Szalai & J. Vinkó (2013) and R. Kotak et al. (2006) are now offset by about 58 days.

A general model of dust formation in SNe has been developed previously using a chemical kinetic approach (A. Sarangi et al. 2018b). In this study, we used the specific ejecta properties that match the optical data of SN 2005af to derive its dust properties. Using that as a reference, we analyze the IR data to distinguish between the dust formed in a pre-explosion wind and post-explosion ejecta. This is the first study where we correlate JWST and Spitzer observations with dust-formation models to derive a consistent dust-evolution scenario in an SN.

2. Rationale of the Study

Here we report the first comprehensive analysis of an SN that connects early- and late-time mid-IR data with unique dust-formation models. We investigate the properties of the dust formed in SN 2005af over ∼2 decades post-explosion, which is reflected in the detections with the JWST MIRI imager. This method enables us to distinguish between the various dust components and their locations, alongside estimating the timing of dust formation.

In our recent surveys of dusty SNe such as SN 2004et, SN 1980K, or SN 1993J (M. Shahbandeh et al. 2023; S. Zsíros et al. 2024; T. Szalai et al. 2025), we stressed the large degeneracies in the location of dust and their chemical compositions, which cannot be uniquely resolved from the analysis of the IR data. In this paper on SN 2005af, we aim to connect the dust evolution in the ejecta and the surrounding medium from the time of explosion through the next two decades. When analyzing the IR data from Spitzer and JWST, the degeneracies on where the dust is located, and if the dust is likely to be silicate-rich or carbon-rich, were resolved with support from the chemical models of dust synthesis based on SN 2005af. In this regard, we shall first derive the theoretical estimates of dust formation in SN 2005af, so we have some references to use in our IR analysis.

The paper is organized as follows. In Section 3, we outline the model of dust formation in SN 2005af, based on SN properties derived from light curve modeling. Thereafter, in Sections 4 and 5, we summarize the optical data from CSP-I and the Keck telescope, and the available IR observations using Spitzer. In Section 6 we discuss the findings of our newly obtained JWST photometric data. In Section 7, we describe the evolution of dust in SN 2005af from 2005 until 2024, which is consistent with all the observations. Finally, in Section 8, we present our findings about the overall physical background of the SN.

3. Chemical Model of the Ejecta

The timescale, composition, and amount of dust produced in an SN depend on the evolution of physical conditions in the ejecta (A. Sarangi et al. 2018b; A. Sarangi 2022). Specifically, the explosion energy, the mass of the ejecta, the chemical abundances, the velocity of the expanding gases, the mass of ^{56}Ni produced, and the clumpiness of the ejecta dictate the scenario of dust formation in SNe.

Modeling the light curve of SN 2005af (Figure 1), these physical parameters of the ejecta have been estimated. Synthetic light curves were calculated using a one-dimensional (1D) hydrodynamical code that simulates the explosion of the SN and produces bolometric light curves (M. C. Bersten et al. 2011). This code has been widely used in the literature to model SN II light curves and derive physical properties (e.g., L. Martinez et al. 2020, 2022a). The stellar models from

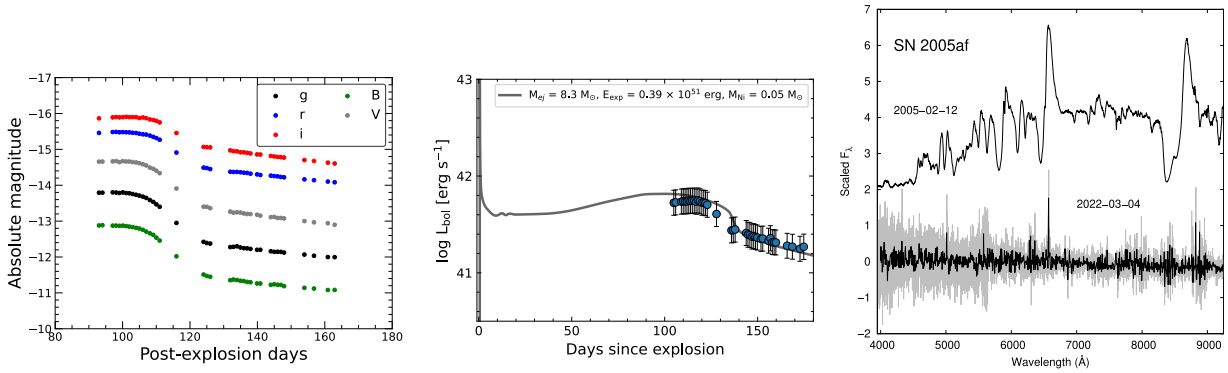

Figure 1. Left: fluxes for the B (0.435 μm), g (0.477 μm), V (0.538 μm), r (0.622 μm), and i (0.761 μm) bands of SN 2005af are presented for the epochs (day 92 to day 163 post-explosion) covered by the CSP-I (J. P. Anderson et al. 2024). Middle: The best-fit light curve model, where the parameters are given in Table 1. Right: two high-resolution optical spectra by Keck/LRIS obtained at day 92 post-explosion, and also at day 6322 post-explosion.

T. Sukhbold et al. (2016) computed with the KEPLER code (T. A. Weaver et al. 1978; S. E. Woosley et al. 2002) were used as pre-SN conditions to initialize the explosion. Then, we estimated the progenitor and explosion properties of SN 2005af by comparing models constructed from different physical properties with the SN bolometric light curve. Therefore, we used the bolometric light curve of SN 2005af previously calculated by L. Martinez et al. (2022b) for the comparison. The estimated physical parameters are reported in Table 1. Using these results, we follow the prescription given by A. Sarangi (2022) to derive the dust masses as a function of time.

Based on the light-curve properties, SN 2005af is proposed to have a relatively low-mass progenitor, with a main-sequence mass of about 10 $M_{\odot}$. This is the first model of dust formation applied to a core-collapse SN originating from such a low-mass progenitor. Previously derived dust formation models were mostly based on SN 1987A (A. Sluder et al. 2018; A. Sarangi 2022), which is not ideal for this scenario.

The ejecta is assumed to consist of an H-rich envelope surrounding an outer H-rich layer and an inner He core. Following the dynamics of SN ejecta (for details, see A. Sarangi 2022) given by J. K. Truelove & C. F. McKee (1999), we find the ejecta core to have a velocity of about 2400 km s^{-1} in this case. The metal-rich part is concentrated in the He core, which is confined within 1400 km s^{-1}. This He-core velocity is considerably slower than models based on SN 1987A presented by A. Sarangi (2022), based on a 20 $M_{\odot}$ star. Slower expansion velocities correspond to more compact ejecta, with higher densities. The distribution of elements in the SN ejecta is shown in Figure 2 in velocity space. Based on the abundances, the ejecta are stratified into O/Si, O/C, and He/C layers (A. Sarangi & I. Cherchneff 2013). The densities (Figure 2) for the clumpy medium are obtained from the light-curve analysis, while the densities of the interclump medium follow the homogeneous density structure given by J. K. Truelove & C. F. McKee (1999). As in A. Sarangi (2022), we consider dust formation only in the clumps. The evolution of the temperature, shown in Figure 2, also varies between the layers (O/Si, O/C, and He/C), with reference to the description by A. Sarangi (2022).

Dust formation in the ejecta of SNe occurs through simultaneous phases of nucleation and condensation. We address the formation of dust in the ejecta of SN 2005af using a nonequilibrium chemical kinetic approach, which was developed in previous studies to account for any core-collapse SNe in general (A. Sarangi & I. Cherchneff 2013, 2015; A. Sarangi et al. 2018b; A. Sarangi 2022). The detailed formalism described by A. Sarangi (2022) is used as the framework in this paper to derive the rate of dust formation in SN 2005af and its distribution inside the ejecta. We consider O-rich dust (silicates and alumina) and C-rich dust (amorphous carbon and silicon carbide).

Table 1
Progenitor and Explosion Properties of SN 2005af Derived from Light-curve Modeling

Progenitor ($M_{\odot}$)	Ejecta ($M_{\odot}$)	$E_{\rm exp}$ (erg s^{-1})	^{56}Ni ($M_{\odot}$)
10.0	8.3	0.39×10^{51}	0.050

The top panel of Figure 3 shows the evolution of dust in the ejecta of SN 2005af. The top panel displays the distribution of dust in velocity space at days 600 and 2900. We find that the O-rich dust, such as silicates, forms rapidly (as early as day 400), and the mass of silicates at day 600 is already 4×10^{-3} $M_{\odot}$. Silicates and alumina form in the inner O/Si-rich core, which in this case is confined only within an expansion velocity of 1200 km s^{-1}. Carbon and silicon carbide form much later, after 1100 days post-explosion. Rapid condensation of carbon dust takes place in the outer He/C-rich layers (velocities between 800 and 1400 km s^{-1}) at that time. We find that, overall, C-rich dust will dominate the dust composition of SN 2005af, with 0.02 $M_{\odot}$ of amorphous carbon dust formed in the ejecta. This is expected to be a characteristic of low-mass progenitors, given their relatively lower mass of the O-rich layer compared to the He-rich layer (A. Sarangi & I. Cherchneff 2013; T. Sukhbold et al. 2016). For the model, the total dust mass is about 0.03 $M_{\odot}$ formed in the metal-rich He core of the ejecta. Molecules such as CO and SiO are abundantly formed in the ejecta, as shown in Figure 4. While CO is the most abundant molecule, SiO depletes rapidly after day 400, leading to the formation of silicate dust.

These theoretical predictions are used in the following sections as a reference when analyzing the IR data for dust composition and location.

4. Optical Data

In this study, we used the optical photometric data of SN 2005af (see Figure 1) in the B (0.435 μm), g (0.477 μm), V (0.538 μm), r (0.622 μm), and i (0.761 μm) bands,

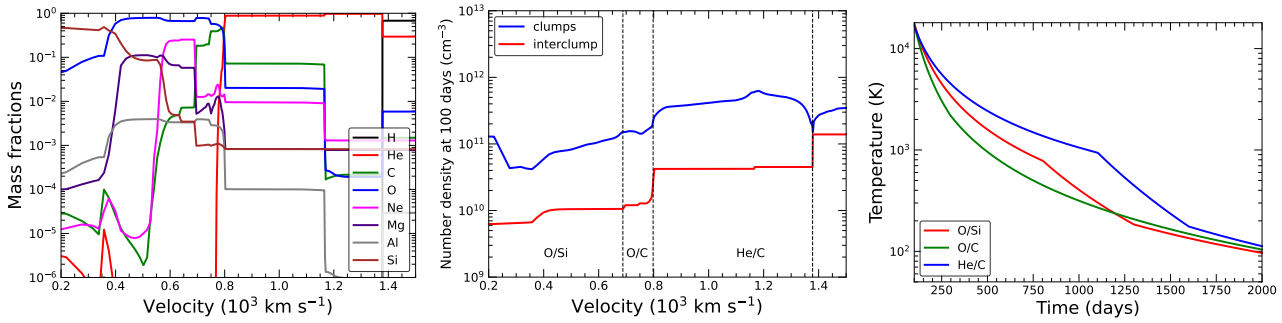

Figure 2. The input conditions for dust-formation modeling in SN 2005af are presented. Elemental abundances (left), gas densities at day 100 (center), and gas temperatures (right) are derived using the formalism adopted by A. Sarangi (2022) and the SN 2005af ejecta parameters derived in Section 3 (see Table 1). The abundances and densities are shown in velocity space. The evolution of gas temperature is shown as a function of time for the O/Si, O/C, and He/C layers.

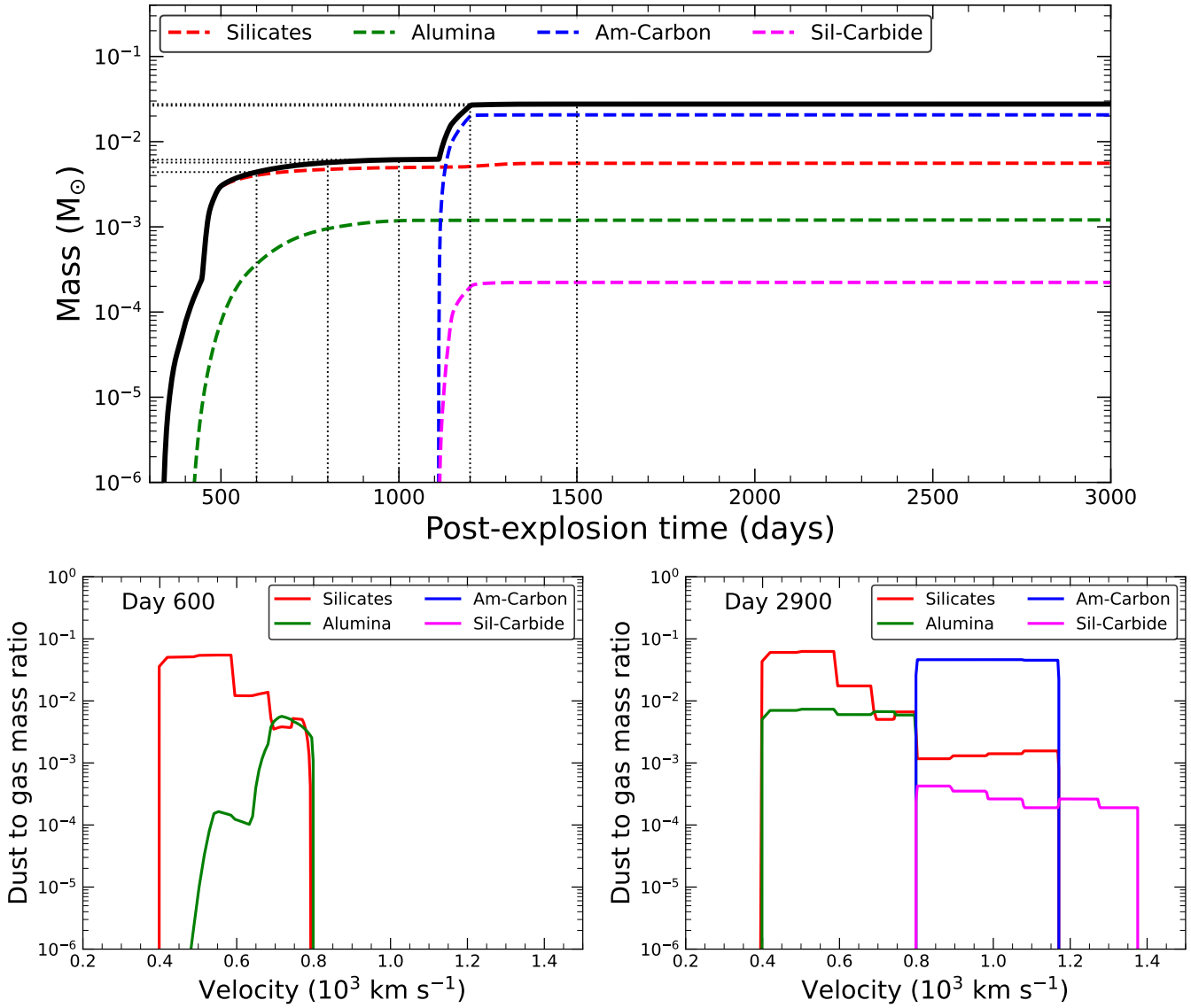

Figure 3. Top: the composition and evolution of dust in SN 2005af, derived from the dust-formation model, is presented. O-rich dust, namely silicates and alumina and C-rich dust, namely amorphous carbon and silicon carbide, are considered. The model suggests steady growth of O-rich dust between days 400 and 800 post-explosion. Amorphous carbon dust forms at a rapid rate after 1100 days, and it becomes the most abundant dust component in the ejecta. Based on this study, we suggest that in SN 2005af, the ejecta are predominantly C-rich in dust. Bottom: the suggested distribution of dust within the ejecta of SN 2005af is shown for day 600, when dust formation has just begun, and for day 2900, when the formation of dust is already saturated. It is evident that O-rich dust is likely to form in the inner regions, while C-rich dust forms in the outer parts of the He core.

corresponding to epochs between 92 and 163 days post-explosion (J. P. Anderson et al. 2024), obtained as part of CSP-I (M. Hamuy et al. 2006). We also present a single unpublished late-time optical spectrum of SN 2005af (Figure 1, right panel) obtained with the Keck Low-Resolution Imaging Spectrometer (LRIS; J. B. Oke et al. 1995) on 2022

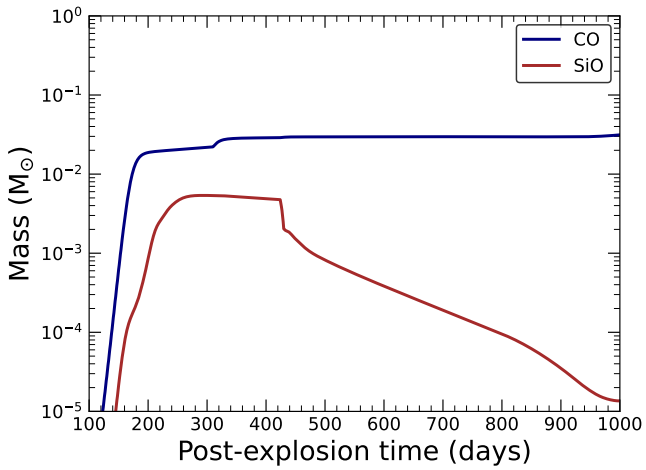

Figure 4. The model predictions for the mass of molecules CO and SiO as a function of post-explosion time in the ejecta of SN 2005af. SiO molecules are considered a tracer and precursor of silicate dust formation (A. Sarangi & I. Cherchneff 2013), while CO molecules remain as the most abundant molecule in the gas.

March 4 (at epoch 6322 days). The spectrum was acquired with the slit oriented at or near the parallactic angle to minimize slit losses caused by atmospheric dispersion (A. V. Filippenko 1982). The LRIS observation utilized the 1″-wide slit, 600/4000 grism, and 400/8500 grating to produce a similar spectral resolving power ($R \approx$ 700–1200) in the red and blue channels.

5. Spitzer Observations

5.1. Photometry

SN 2005af was imaged several times with the Spitzer Infrared Array Camera (IRAC) and Multiband Imaging Photometer for Spitzer (MIPS) between 2005 and 2019 (Figure 5). As noted in Section 1, we have updated the explosion epoch to be MJD 53320.8 based on C. P. Gutiérrez et al. (2017); hence, the epochs mentioned previously by T. Szalai & J. Vinkó (2013) and R. Kotak et al. (2006) are offset (increased) by 58 days.

For SN 2005af, the early evolution, R. Kotak et al. (2006) and R. Kotak (2008) presented mid-IR observations. R. Kotak et al. (2006) reported the first identification of the SiO molecule in a Type IIP SN, based on observations from day 272. T. Szalai & J. Vinkó (2013) presents the full Spitzer data set of SN 2005af up to ∼998 post-explosion. That study, however, is based on the analysis of the post basic calibrated data—applying simple aperture photometry with a 5–12–20 configuration in native 1.″2 IRAC pixels—which results in a $\gtrsim$10% photometric uncertainty. Thus, for our current study, we repeated the whole analysis: we downloaded the basic calibrated data of the SN from the Spitzer Heritage Archive and thoroughly reanalyzed all the early-time archival Spitzer IRAC data (but we did not use the MIPS images because of their spatial and spectral limitations). During the photometric reduction, we performed overlap correction and mosaicing of the frames with `MOPEX` (D. Makovoz & I. Khan 2005). We invoked the task `APEX` User List Multiframe, with the absolute SN position as input, to extract the flux via fitting of the point-response function for each epoch. Note that the formal uncertainties of the fluxes (based on the signal-to-noise ratio) are implausibly low. Thus, to obtain more realistic error measurements, we used the uncertainties derived from an alternative aperture-photometry analysis (described by O. D. Fox et al. 2011) conducted on both the source and the background. With this method, we are able to sample the background of just the SN and eliminate the effect of bright sources in its vicinity. The results of the Spitzer/IRAC photometry of SN 2005af are presented in Table 2. As can be seen, the new photometry is in good agreement with the values published in T. Szalai & J. Vinkó (2013) at the first two epochs; however, there are larger differences at later times (probably because of the too large aperture size used in the previous study), which confirms our strategy on revising the previously published photometry.

5.2. Spectroscopy

SN 2005af has also been observed with the Spitzer Infrared Spectrograph (IRS) at four epochs (R. Kotak et al. 2006; R. Kotak 2008) during its early evolution (at days 125, 272, 629, and 864 after explosion). We downloaded the four available IRS spectra of SN 2005af from the Combined Atlas of Sources with Spitzer IRS Spectra (CASSIS)[24] database (V. Lebouteiller et al. 2011). We used the best flux-calibrated spectra, respectively, following the guidelines provided by the CASSIS recommendations.

6. JWST/MIRI Imaging

As part of the Cycle 1 General Observers (GO) 2666 program[25] (PI O. D. Fox), we obtained images of SNe 2005af with the JWST Mid-Infrared Instrument (MIRI) on 2023-07-21 (6826 days post-explosion). The observations (DOI: 10.17909/5aw1-qg12) were acquired in the F560W, F1000W, F1130W, F1280W, F1500W, F1800W, F2100W, and F2550W filter bands, using the FASTR1 readout pattern in the FULL array mode and a 4-point extended source dither pattern (Figure 6). A description of our detailed calibration process of the JWST/MIRI images was recently published by M. Shahbandeh et al. (2023). We use the JWST HST Alignment Tool (JHAT; A. Rest et al. 2023) to align JWST and HST images of the fields of the host galaxy with each other.

To measure the fluxes of SN 2005af on JWST/MIRI images, we followed the method described in detail by M. Shahbandeh et al. (2023). We performed point spread function (PSF) photometry on background-subtracted level-two data products using `WebbPSF` (M. D. Perrin et al. 2014) implemented in the `space-phot` package[26] (J. Pierel 2024). In order to calibrate the flux, we applied flux offsets by measuring the PSF of all the stars in the field and comparing them to the corresponding catalogs created by the pipeline. The fluxes of all four dithers of each filter were then averaged. The final results of JWST/MIRI photometry of SN 2005af are presented in Table 3.

7. Evolution of Dust

To describe the dust formation history of the SN we fit its mid-IR emission. The distance of the SN was taken as 3.9 Mpc

[24] https://cassis.sirtf.com/
[25] https://www.stsci.edu/jwst/science-execution/program-information?id=2666
[26] https://zenodo.org/records/12100100

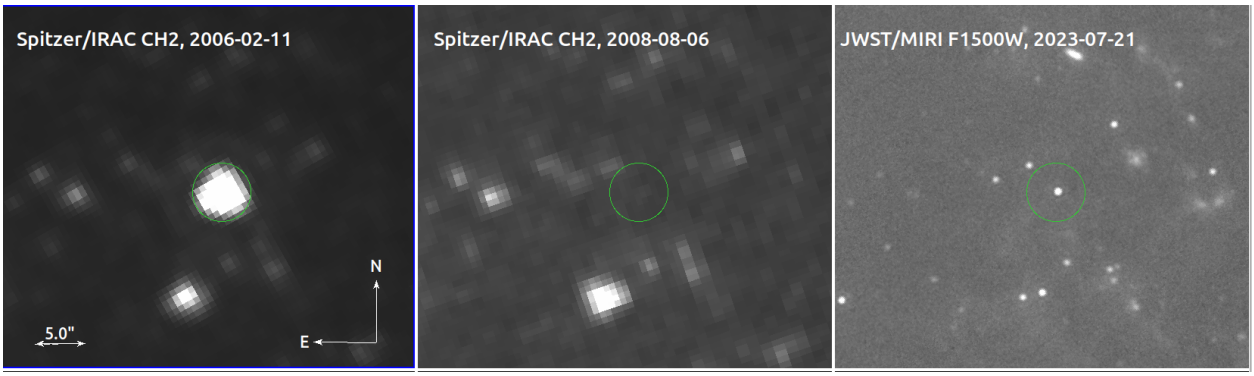

Figure 5. Left and Middle: Spitzer IRAC images of SN 2005af taken on 2006 February (458 days post-explosion) and 2008 August (1363 days post-explosion) (T. Szalai & J. Vinkó 2013) Right: JWST/MIRI image of SN 2005af taken in 2023 July (6826 days post-explosion) in filter band F1500W.

Table 2
The Results of the Spitzer/IRAC Photometry of SN 2005af

MJD (days)	Epoch (days)	$F_{3.6}$ (μJy)	$F_{4.5}$ (μJy)	$F_{5.8}$ (μJy)	$F_{8.0}$ (μJy)
53573.3	252.5	3772 ± 100	17940 ± 216	9284 ± 147	6968 ± 112
…	…	*(3849 ± 104)*	*(17984 ± 211)*	*(9014 ± 151)*	*(7283 ± 138)*
53778.9	458.1	858 ± 44	3210 ± 88	2139 ± 59	4448 ± 80
…	…	*(956 ± 52)*	*(3348 ± 91)*	*(2192 ± 75)*	*(4870 ± 115)*
53955.1	634.3	136 ± 13	407 ± 27	848 ± 35	1769 ± 38
…	…	*(254 ± 28)*	*(492 ± 35)*	*(972 ± 52)*	*(2193 ± 78)*
54151.12	830.3	13 ± 3	25 ± 4	91 ± 5	256 ± 8
…	…	*(135 ± 22)*	*(112 ± 18)*	*(236 ± 29)*	*(774 ± 55)*

Note. Numbers marked with italic show the photometric values previously published in T. Szalai & J. Vinkó (2013).

(A. V. Filippenko & R. J. Foley 2005; C. Jacques & E. Pimentel 2005; R. Kotak et al. 2006). The nature and evolution of dust in SN 2005af from 2 months post-explosion, until 18.7 yr, is estimated using Spitzer and JWST data summarized above. We applied both blackbody and analytical dust models. The parameters are listed in Table 4. We have used silicates and amorphous carbon dust as the two main dust types, whose optical properties are given by B. T. Draine & A. Li (2007) and V. Zubko et al. (2004). Here we have derived the amount of pre-existing dust in the CSM, which was formed in the pre-explosion winds, in addition to the amount of newly formed dust in the SN ejecta, post-explosion. For simplicity, we have chosen all grains to be of spherical shape and 0.1 μm radius, as also previously assumed by A. Sarangi (2022) and M. Shahbandeh et al. (2023). To resolve the degeneracies while fitting the IR data, such as when multiple scenarios can produce a reasonably good fit, we have relied on the physical models (Section 3) for determining the most likely scenario.

7.1. Dust Emission and Geometry

We estimated the mass and temperature of dust based on the assumptions that (a) the SN ejecta and the CSM have a spherically symmetric geometry, (b) dust at a given location has an identical temperature, and (c) the dust grains are of identical size a of 0.1 μm. As argued in previous studies (O. D. Fox et al. 2010; A. Sarangi 2022; M. Shahbandeh et al. 2023), in the mid-IR regimes, grain size distributions do not have a significant impact on the fluxes.

At a given time, the flux produced by dust of mass m_d and temperature T_d is given by

$$F_\lambda(\lambda, T_d) = \frac{4\, m_d \quad k(\lambda, a)\, \pi B_\lambda(\lambda, T_d) P_{\rm esc}(\lambda)}{4\pi D^2}, \qquad (1)$$

where D is the distance of the SN, B is the Planck function, k (λ, a) is the mass absorption coefficient, and $P_{\rm esc}(\lambda)$ is the escape probability of a photon from the dust cloud. We have used the absorption coefficients $k(\lambda)$ for silicates and amorphous carbon dust from B. T. Draine & A. Li (2007) and V. Zubko et al. (2004), respectively, similar to our recent studies (A. Sarangi 2022; M. Shahbandeh et al. 2023; S. Zsíros et al. 2024). The escape probability of a photon of wavelength λ from a dusty sphere of uniform temperature (E. Dwek & R. G. Arendt 2015; A. K. Inoue et al. 2020) is given by

$$P_{\rm esc}(\lambda) = \frac{3}{4\tau}\left[1 - \frac{1}{2\tau^2} + \left(\frac{1}{\tau} + \frac{1}{2\tau^2}\right)e^{-2\tau}\right]. \qquad (2)$$

The optical depth $\tau(\lambda)$ of a sphere of radius R with uniform dust density is given by

$$\tau(\lambda) = \frac{3 m_d k(\lambda)}{4\pi R^2}. \qquad (3)$$

If the dust is distributed in a spherical shell of inner and outer radii R_1 and R_2 (respectively), the optical depth is given by

$$\tau(\lambda) = \frac{3 m_d k(\lambda)}{4\pi (R_2^2 + R_1 R_2 + R_1^2)}. \qquad (4)$$

When the mass of dust is large, the respective optical depth is large as well. In that case, the escape probability at any

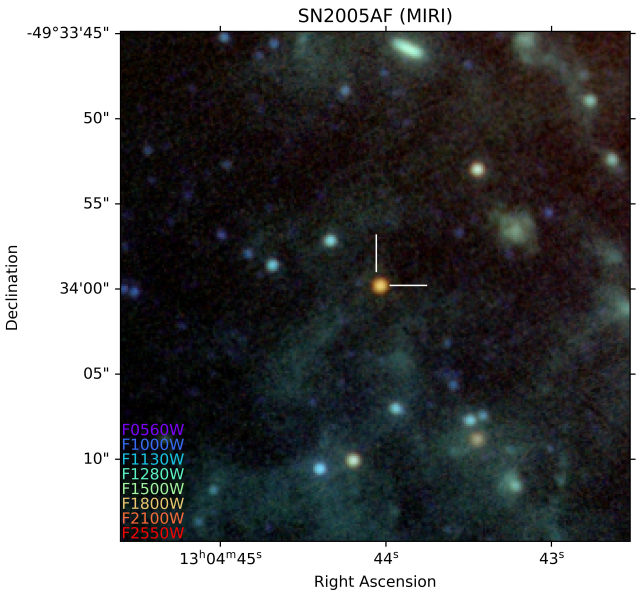

Figure 6. JWST/MIRI composite image of SN 2005af, taken on 2023 July 21, which is 6826 days post-explosion. The white tick marks show the position of the supernova.

Table 3
JWST/MIRI Photometry of SN 2005af

Filters	AB Mag	F_ν (μJy)
F560W	<22.03	<5.6
F1000W	22.01 ± 0.10	5.7 ± 0.6
F1130W	20.80 ± 0.10	17.3 ± 1.5
F1280W	19.80 ± 0.03	43.6 ± 1.1
F1500W	18.89 ± 0.01	100.7 ± 1.4
F1800W	18.32 ± 0.02	171.0 ± 2.9
F2100W	17.95 ± 0.02	240.2 ± 5.2
F2550W	16.93 ± 0.03	613.7 ± 17.8

Note. All observations were taken on 2023 July 21, that is 6826 days post-explosion.

given wavelength is small, since the IR radiation from the dust is self-absorbed within the cross-section of the dusty sphere. In the other extreme scenario, where the mass of dust is small, representing an optically thin medium, the escape probability is close to 1.

We have used Equation (1) to fit the obtained IR fluxes of SN 2005af, as described below. The `python scipy` library `curve_fit` was used for fitting and error analysis.

7.2. Day 125

At day 125, the spectrum is largely dominated by the optical emission from the SN photosphere. We combined the optical photometric data obtained from CSP-I (Figure 1) at epoch 125 post-explosion, along with the Spitzer spectrum at the same epoch. The optical part of the data was fit using a blackbody spectrum. The blackbody component is of temperature 3459 K and radius 2.1×10^{15} cm. In addition, we find the presence of a significant excess in the near-IR and mid-IR, dominating over the optical blackbody (Figure 7, Table 4). Such early epochs are not suitable for dust condensation in the hot ejecta, as seen in Section 3 (A. Sarangi et al. 2018b). A. Pereyra et al. (2006) suggests a possibility for the presence of a dusty CSM in SN 2005af. We consider this emission to be from the dust in the CSM, which was formed in the winds prior to the explosion. In Type II-P SNe, the CSM is formed by the winds blown from the H-rich outer envelope of the massive star, where the C/O ratio is smaller than 1 (T. Sukhbold et al. 2016). O-rich dust such as silicates is expected in such environments (V. Lebouteiller et al. 2012; J. S. Clark et al. 2013). We find the mass of silicate to be about $2.9 \times 10^{-3}\ M_\odot$, at 179 K. At this early epoch, such low dust temperatures require the dust to be present at large distances from the SN. Our calculation suggests the dust to be around 2–4 $\times$ 10^{17} cm from the photosphere, to match this temperature. In comparison, if we assume a forward shock velocity of 5000 km s^{-1}, the SN shock will be only at 5×10^{15} cm at this epoch. Therefore, the dust is very likely to be pre-existing in the CSM. Ejecta dust, if present within the photosphere at these early epochs, is supposed to be much hotter.

7.3. Day 272

Day 272 shows a trend similar to that of day 125, where the combined Spitzer/IRAC fluxes and the IRS spectrum show the presence of an IR-excess (Figure 7, Table 4). In sync with the findings of day 125, we report that this is a pre-existing component of dust in the CSM, which gives rise to the IR-excess. We do not expect significant dust condensation at such early times. However, due to the lack of optical data and the poor quality of the obtained Spitzer spectrum, our fit is not very reliable. The temperature of the optical blackbody was obtained to be 2400 K, and a radius of 1.6×10^{15} cm. We find the mass of silicate dust to be $\sim 2.0 \times 10^{-3}\ M_\odot$, at 157 K. Like in the case of day 125, this dust temperature corresponds to a distance of 2×10^{17} cm, while the SN shock is expected to only be around 10^{16} cm at this epoch. On day 272, molecular emission from SiO was detected in its fundamental band in the range 7.9–9 μm, which is a precursor to dust condensation in the ejecta (R. Kotak et al. 2006; A. Sarangi & I. Cherchneff 2013). Note that according to our models, the O-rich dust forms rapidly around day 400. A part of the mid-IR spectrum at this epoch is therefore expected to have some contribution from molecular lines as well.

Importantly, R. Kotak et al. (2006) analyzed the same Spitzer data but did not report the presence of dust emission in the spectra at either day 125 (day 61 in R. Kotak et al. 2006) or day 272 (day 214 in R. Kotak et al. 2006). We agree that atomic and molecular line emission from CO and SiO in the ejecta may dominate the spectra until 9.5 μm, as noted by R. Kotak et al. (2006). We did not include molecular emission in our fit. However, we report evidence for a dust component in the extended CSM gas, which contributes to an IR excess in the spectra at both epochs. This excess is most significant at longer wavelengths beyond 10 μm and does not conflict with the presence of molecules. In fact, our dust-evolution scenario supports the appearance of SiO molecules at day 272, which subsequently led to the formation of silicate dust in the ejecta at later epochs. The mid-IR data from day 272 is noisy. But since we find compelling evidence of an IR excess at day 125, arguably originating from pre-existing dust, we suggest that the component should also be present at day 272.

Table 4
Best-fit Parameters and Percentage Errors for all Analyzed IR Observations of SN 2005af Spanning Over two Decades, Compared to Model Results

Parameter	Unit	Optical BB (error%)	Pre-existing CSM Dust (error%)	Ejecta Dust (error%)	Ejecta Model
Day 125 Spitzer/IRS					
BB radius	cm	2.1×10^{15} (0.1)	⋯	⋯	⋯
Dust type	⋯	⋯	Silicate	⋯	⋯
Temperature	K	3459 (0.4)	179 (8)	⋯	⋯
Dust mass	$M_\odot$	⋯	2.9×10^{-3} (38)	⋯	⋯
Dust velocity	km s^{-1}	⋯	⋯	⋯	⋯
Day 272 Spitzer/IRS + IRAC					
BB radius	cm	1.6×10^{15} (0.1)	⋯	⋯	⋯
Dust type	⋯	⋯	Silicate	⋯	⋯
Temperature	K	2400 (6.9)	157 (51)	⋯	⋯
Dust mass	$M_\odot$	⋯	2.0×10^{-3} (246)	⋯	⋯
Dust velocity	km s^{-1}	⋯	⋯	⋯	⋯
Day 629 Spitzer/IRS + IRAC					
Dust type	⋯	⋯	Silicate	Silicate	Silicate
Temperature	K	⋯	129 (5)	459 (6)	⋯
Dust mass	$M_\odot$	⋯	6.5×10^{-3} (23)	3.0×10^{-3} (min.)	4.2×10^{-3}
Dust velocity	km s^{-1}	⋯	⋯	1290 (10)	810
Day 830 Spitzer/IRAC + Day 864 IRS					
Dust type	⋯	⋯	Silicate	Silicate	Silicate
Temperature	K	⋯	106 (95)	349 (31)	⋯
Dust mass	$M_\odot$	⋯	6.0×10^{-3}	2.2×10^{-3} (min.)	4.8×10^{-3}
Dust velocity	km s^{-1}	⋯	⋯	800 (79)	814
Day 6826 (18.7 yr) JWST/MIRI					
Dust type	⋯	⋯	⋯	Carbon, Silicate	Carbon, Silicate
Temperature	K	⋯	⋯	108 (76), 80 (max.)	⋯
Dust mass	$M_\odot$	⋯	⋯	0.0143 (64), 1.8×10^{-3}	0.021, 4.7×10^{-3}
Dust velocity	km s^{-1}	⋯	⋯	1250 (1100), 706	1190, 805

7.4. Day 629

On day 629, we find the presence of two distinct IR components, hot and cold (Figure 7, Table 4). The cold silicate component at 129 K with a mass of $\sim 6.0 \times 10^{-3}\,M_\odot$ is aligned in temperature with the pre-existing dust that produces the IR excess at days 125 and 272. Even though the CSM dust mass should not increase, a larger mass estimated from the spectra may be attributed to the increase in the echo due to the effect of the light-travel time (E. Dwek 1985; E. Dwek et al. 2021).

Most core-collapse SNe are known to form dust by day 629 (L. B. Lucy et al. 1989; A. Sarangi et al. 2018b), and the chemical model of SN 2005af in Section 3 predicts the formation of silicate dust of $\sim 4.2 \times 10^{-3}\,M_\odot$ in the ejecta. Moreover, the detection of SiO molecules (R. Kotak et al. 2006; P. Crowther & S. Smartt 2007) also suggests the formation of silicate dust in this SN. However, the spectrum does not show any notable peak around 9.7 μm, which is characteristic of silicate dust. We find that, if at least $3.0 \times 10^{-3}\,M_\odot$ of silicate dust is formed in the O-core of the ejecta expanding at $\sim$1290 km s^{-1} (assuming homologous expansion), the emission from that hot, newly formed dust ($\sim$459 K) can fit the observed spectrum. A blackbody radius for this spectrum results in a velocity of $\sim$1200 km s^{-1} at day 629. Hence, an emission from optically thick silicate with a similar velocity can well explain the origin of the hot component of the IR spectrum. Owing to the dust being optically thick (Equation (3)), it suppresses the 9.7 and 18 μm silicate features in the emission spectrum (E. Dwek & R. G. Arendt 2015; A. Sarangi 2022). The dust mass is quite in agreement with the theoretical model, where $4.2 \times 10^{-3}\,M_\odot$ of dust is found to have formed inside a sphere of $\sim$810 km s^{-1}. Technically, there is no threshold mass that defines when the dusty sphere becomes optically thick, since optical depths are wavelength dependent. We find in this case that any dust mass larger than $3.0 \times 10^{-3}\,M_\odot$ does not change the total IR luminosity, and hence we can consider it as a reasonable lower limit for the dust mass in the ejecta.

7.5. Days 830 and 864

The IRAC fluxes on day 830 and the IRS spectrum on day 864 are combined in a single analysis. However, the data are subject to large uncertainties. The silicate dust in the ejecta is taken as responsible for the hot IR emission. For the best scenario, we find silicates in the ejecta have a mass lower limit of $2.2 \times 10^{-3}\,M_\odot$ and a temperature of 349 K. The pre-existing dust mass remains unaltered. Given the large uncertainties in the observed fluxes, we suggest the reader to only consider the trend and not stress the absolute values from the fit at this epoch.

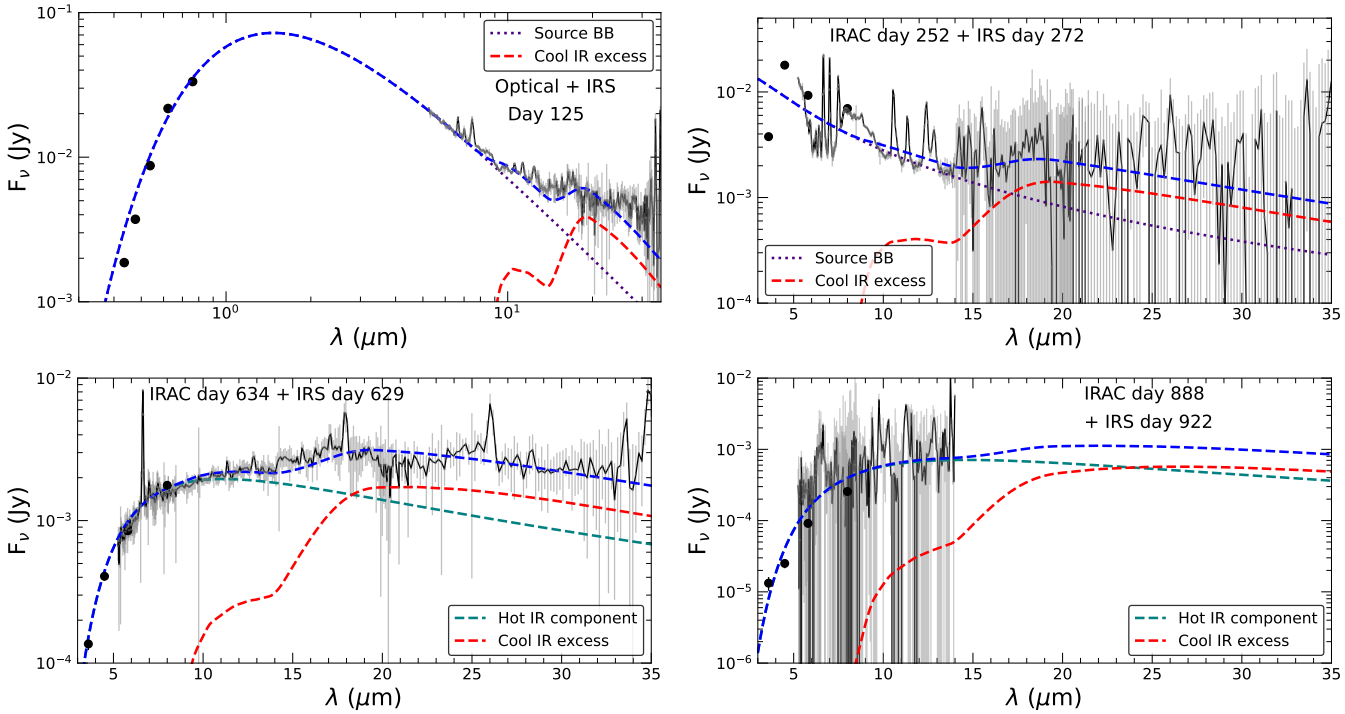

Figure 7. The best-fit cases for four epochs of observation by Spitzer through IRAC imaging (solid black circles) and IRS spectroscopy. For day 125, we combined the optical data from CSP-I with the Spitzer spectrum. The epochs of day 125 and day 272 (+IRAC day 252) were fit using a blackbody (in dotted, purple line) for the optical component, along with a cool IR component (dashed, red line) from dust (sum of the two components given in blue). For epoch 629 (+IRAC day 634) and epoch 806 (+IRAC day 830), we assumed a combination of hot (in green) and cool IR (red) components. We suggest that the cool IR component for all the cases originates from some pre-existing dust in the circumstellar matter, which was formed in the winds of the progenitor before the explosion. The hot IR component is attributed to emission from newly formed dust in the ejecta. See Table 4 for the fitting parameters and Section 7 for a detailed description of the scenario.

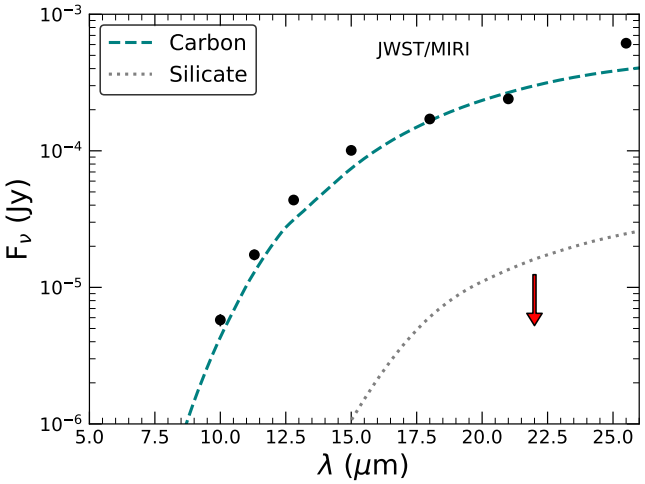

Figure 8. The best-fit model is presented for mid-IR fluxes (data given in Table 3) of SN 2005af obtained through JWST/MIRI, 6826 days post-explosion. We find that, at this epoch, dust is predominantly C-rich in composition. See Section 7.6 and Table 4 for the description.

7.6. Day 6826—Year 18.7 (JWST/MIRI)

SN 2005af was observed by JWST in 2023, about 19 yr after the explosion and ∼16 yr from when it was last observed with Spitzer. The fluxes in the MIRI bands (10.0, 11.3, 12.8, 15.0, 18.0, 21.0, and 25.5 μm) do not show any noticeable spectral features (Figure 8). We find that the data fit well with an amorphous carbon component, while silicate dust is not a good candidate given its strong features at 9.7 and 18 μm. For clarity of understanding, in the first few years after the explosion, the expanding SN ejecta remain very compact in radius; hence, a small mass of dust makes it optically thick at mid-IR wavelengths. It is difficult to distinguish between carbon and silicate dust at that point, since the silicate features are suppressed due to large opacities. However, at later times, such as 19 yr, the ejecta expand to a large radius, and hence the mid-IR optical depths are reduced considerably. At these epochs, it is possible to determine the likely dust composition. We find a mass of carbon dust to be 0.014 $M_\odot$ at a temperature of 108 K (Figure 8, Table 4). The IR luminosity at this epoch is $\sim 10^{38}$ erg s^{-1}. The velocity of the dusty sphere is found to be 1250 km s^{-1}. However, owing to the featureless nature of the fluxes, the velocity is not well constrained, incurring large uncertainties. The model presented in Section 3 predicts the mass of carbon dust to be 0.02 $M_\odot$, where amorphous carbon is the most abundant dust type in SN 2005af. The velocity of the dusty region (1190 km s^{-1}) is also in agreement with the fit to the observed data.

At the Spitzer epochs, we considered the presence of silicate dust in the ejecta. When analyzing the JWST fluxes, we find that carbon and silicates may coexist in the ejecta; however, the silicate must be cooler than the amorphous carbon dust. The best-fit temperature for carbon is 108 K, and the maximum possible temperature for silicates is ∼80 K. In Figure 8, we show the maximum silicate contribution with a downward arrow. The likely scenario where carbon and silicate dust are at different temperatures cannot be addressed based on the data alone. With regard to the stellar structure (S. E. Woosley et al. 1989; T. Rauscher et al. 2002; T. Sukhbold et al. 2016) and the dust-formation zones, as presented in Section 3 (A. Sarangi & I. Cherchneff 2013; A. Sarangi 2022), it has been predicted that carbon dust forms in the outer He-rich layers, while O-rich silicate dust forms essentially in the O-core. Analyzing the

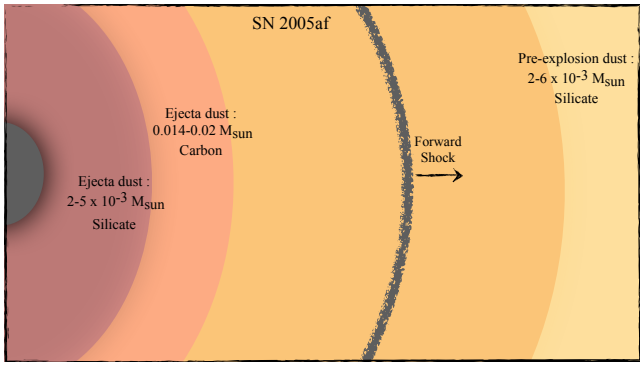

Figure 9. A summary of the location, composition, and mass of dust in SN 2005af two decades after the explosion is presented in a schematic diagram (see Sections 7 and 8 for details). The inner O/Mg/Si shell, marked in brown, is where silicate dust is formed. The He/C shell, marked in orange, is the site for amorphous carbon dust formation. The dusty region of the CSM, hosting the surviving pre-explosion dust, is marked in yellow.

JWST data from SN 2004et and SN 2017eaw, it has been concluded that the temperature of the ejecta dust after a few years is controlled by heating from an external forward shock (M. Shahbandeh et al. 2023). We find that 0.014 $M_\odot$ of carbon dust in the outer shell at velocities of 800–1200 km s^{-1} has optical depths τ (0.1 μm), τ (0.3 μm), and τ (0.6 μm) of 2.1, 2.6, and 2.9, respectively (Equation (4)). Therefore, if silicate dust is internal to carbon dust and is heated by an external shock (see Figure 9), we can justify the difference in temperature. In the future, we will construct a complete radiative-transfer model to calculate the variation of dust temperatures between zones.

We note that there is an excess at the longest MIRI filter of 25.5 μm, over our fit with 0.014 $M_\odot$ of carbon dust at 106 K, as visible in Figure 8. This indicates that there might be larger masses of cold dust that are not detected by JWST. SN 1987A was found to host about 0.5 $M_\odot$ of dust at a temperature of 17–23 K (M. Matsuura et al. 2015). The dust mass we detected by JWST, by analyzing the mid-IR emission, is a lower limit of the dust present in SN 2005af.

7.7. Summary of the Dust Evolution

In Figure 9, we present a simple schematic scenario of the location, type, and amount of dust that is present in SN 2005af 20 yr post-explosion. This is the first study where the dust formed in the CSM prior to the explosion and newly formed dust in the ejecta are differentiated, combining modeling and observations. We find amorphous carbon to be the dominant dust species in the ejecta, constituting almost 80% of the total dust. This is justified if SN 2005af was indeed a low-mass progenitor of about 10 $M_\odot$ while on the main sequence. Such stars are predicted to have a very low mass O-core at the time of explosion (T. Rauscher et al. 2002; T. Sukhbold et al. 2016). However, silicate dust is the first to form in the ejecta, while carbon dust forms after 1000 days. The total amount of dust produced, combining the ejecta (0.019 $M_\odot$) and the CSM (3×10^{-3} $M_\odot$), is about 0.022 $M_\odot$. The pre-explosion CSM dust is expected to encounter the forward shock and be destroyed or reprocessed through it.

7.8. An Alternate Scenario

When correlating the IR fluxes at different epochs to derive the evolution of dust in an SN, there are several degeneracies in the assumed physical parameters that cannot be resolved solely through the fitting of the data. Specifically, the location of the dust (if it is pre-existing or newly formed after explosion), the shape of the dusty sphere or shell, and the relative compositions of different dust types, among other factors, often remain somewhat uncertain. To account for this, there often appear to be multiple scenarios that may all fit the data (M. Shahbandeh et al. 2023; S. Zsíros et al. 2024). In this paper, for SN 2005af, we have presented (summarized in Figure 9) the most suitable picture which agrees with data as well as the chemical models.

In an alternative scenario, the IR spectrum at day 629 and the JWST fluxes at 19 yr can both be fitted using only amorphous carbon dust with mass $\sim 10^{-3}$ $M_\odot$ (or larger) and 0.015 $M_\odot$, respectively. In this picture, silicate dust is not formed in the ejecta at all. However, the presence of SiO lines on day 272 supports the formation of silicate dust. In addition, detection of Ne and Ar lines indicates that the ejecta should have reasonable O-rich and Si-rich layers where silicate dust is known to form (R. Kotak et al. 2006; P. Crowther & S. Smartt 2007; A. Sarangi & I. Cherchneff 2013). Theoretical models suggest that carbon dust formation is delayed owing to the overabundance of He^+ ions in the C-rich layers. Based on these conditions, we support the picture where the ejecta of SN 2005af form both silicates and carbon dust, with silicate dust forming earlier than carbon. We acknowledge that in a special case, if the He-rich layer cools down much faster than the inner O-rich part of the ejecta, we may find C-dust to form within the first two years as well.

8. Discussion

We report that even after 18 yr post-explosion, SN 2005af remains bright in the mid-IR, with a total IR luminosity $\sim 2.7 \times 10^4$ $L_\odot$. The SN ejecta host dust at a temperature of about 100 K at this epoch. In comparison, the mid-IR luminosities of SN 2004et and SN 1980K were found to be 2.2×10^5 $L_\odot$ and 6.3×10^4 $L_\odot$, respectively (M. Shahbandeh et al. 2023; S. Zsíros et al. 2024). The dust temperatures are also found to be lower in SN 2005af with respect to ~150 K reported for SN 2004et and SN 1980K.

As in the cases of SN 2004et and SN 2017eaw (M. Shahbandeh et al. 2023), we argue that the late-time IR fluxes result from heating of the dust by the power generated by the forward shock and CSM interaction. In the absence of suitable optical data at such late epochs (the Keck spectrum at 18 yr shown in Figure 1 does not reveal much about the current state of the SN), we can only calculate a realistic upper limit on the shock power that may heat the dust. Assuming a standard mass-loss rate of 10^{-6} $M_\odot$ yr^{-1}, wind velocity of 10 km s^{-1}, and shock velocity of 5000 km s^{-1}, the mechanical shock power can be calculated to be $\sim 10^6$ $L_\odot$ (C. Fransson et al. 2014; A. Sarangi et al. 2018a). This is sufficient to be assumed as the heating source responsible for the mid-IR fluxes.

There is not much information available about the CSM of SN 2005af. Light-curve models suggest that the progenitor may have lost ~0.33 $M_\odot$ of its H-envelope through mass loss in its entire red supergiant phase. There is no significant evidence for the presence of dense CSM anywhere close to the

star. Our analysis suggests that there is at least $2 \times 10^{-3}\,M_{\odot}$ of dust in the CSM that has survived the explosion. In addition, there is an upper limit for the distance of the CSM dust, based on the dust temperatures of 180–150 K between days 100–250. The nature of mass loss may also affect the CSM dust, which is not constrained by observations. In a future study, we shall formulate a model for the IR echo from the CSM dust at early times to account for the geometry of the pre-existing dust and the CSM.

The final mass of dust is between 0.02–0.03 $M_{\odot}$ in SN 2005af. This compares well with SN 2004et, where the estimated mass is 0.01–0.05 $M_{\odot}$ (M. Shahbandeh et al. 2023). In SN 1980K, the mass was found to be an order of magnitude smaller (S. Zsíros et al. 2024). Here, our main focus is on the degeneracies between the location of dust and the chemical type of dust. Apart from spatially resolved very nearby objects like SN 1987A, this is the first study that differentiates between SN dust formed prior to the explosion and post-explosion. Moreover, we also, for the first time, present a model of dust formation in a low-mass SN progenitor ($\sim$10 $M_{\odot}$ at main sequence).

As concluding remarks, we confirm that the metal-rich core of SN ejecta is a very suitable site for dust formation. Based on our dust-formation model results, the dust-to-metal percentage in the ejecta is found to be $\sim$12%. Comparing the model with mid-IR fluxes from JWST, we suggest that carbon and silicate dust components may remain in the ejecta at different temperatures. We report that SN 2005af produced predominantly C-rich dust in the ejecta and O-rich dust in the pre-explosion winds.

Acknowledgments

We acknowledge funding from NASA/JWST grant GO-2666. A.S. is thankful for the support by a grant from VILLUM FONDEN, Denmark (PI Jens Hjorth) (project number 16599) and the Department of Science and Technology (DST), Gov. of India. S.Z. is supported by the ÚNKP-23-4-SZTE-574 New National Excellence Program of the Ministry for Culture and Innovation from the source of the National Research, Development and Innovation Fund, Hungary. A.V.F. is grateful for financial support from the Christopher R. Redlich Fund, Arthur Folker, Tom and Dana Grogan, Stan Schiffman, Richard Sesler, and many other donors. I.D.L. acknowledges funding from the Belgian Science Policy Office (BELSPO) through the PRODEX project "JWST/MIRI Science exploitation" (C4000142239) and funding from the European Research Council (ERC) under the European Union's Horizon 2020 research and innovation program DustOrigin (ERC-2019-StG-851622).

ORCID iDs

Arkaprabha Sarangi https://orcid.org/0000-0002-9820-679X
Szanna Zsíros https://orcid.org/0000-0001-7473-4208
Tamás Szalai https://orcid.org/0000-0003-4610-1117
Laureano Martinez https://orcid.org/0000-0003-0766-2798
Melissa Shahbandeh https://orcid.org/0000-0002-9301-5302
Ori D. Fox https://orcid.org/0000-0003-2238-1572
Schuyler D. Van Dyk https://orcid.org/0000-0001-9038-9950
Alexei V. Filippenko https://orcid.org/0000-0003-3460-0103
Melina Cecilia Bersten https://orcid.org/0000-0002-6991-0550
Ilse De Looze https://orcid.org/0000-0001-9419-6355
Chris Ashall https://orcid.org/0000-0002-5221-7557
Tea Temim https://orcid.org/0000-0001-7380-3144
Jacob E. Jencson https://orcid.org/0000-0001-5754-4007
Armin Rest https://orcid.org/0000-0002-4410-5387
Dan Milisavljevic https://orcid.org/0000-0002-0763-3885
Luc Dessart https://orcid.org/0000-0003-0599-8407
Eli Dwek https://orcid.org/0000-0001-8033-1181
Nathan Smith https://orcid.org/0000-0001-5510-2424
Samaporn Tinyanont https://orcid.org/0000-0002-1481-4676
Thomas G. Brink https://orcid.org/0000-0001-5955-2502
WeiKang Zheng https://orcid.org/0000-0002-2636-6508
Geoffrey C. Clayton https://orcid.org/0000-0002-0141-7436
Jennifer Andrews https://orcid.org/0000-0003-0123-0062

References

Anand, G. S., Lee, J. C., Van Dyk, S. D., et al. 2021, MNRAS, 501, 3621
Anderson, J. P., Contreras, C., Stritzinger, M. D., et al. 2024, A&A, 692, A95
Andrews, J. E., Gallagher, J. S., Clayton, G. C., et al. 2010, ApJ, 715, 541
Arendt, R. G., Dwek, E., Bouchet, P., et al. 2020, ApJ, 890, 2
Bersten, M. C., Benvenuto, O., & Hamuy, M. 2011, ApJ, 729, 61
Bouchet, P., & Danziger, I. J. 1993, A&A, 273, 451
Cherchneff, I. 2013, in Betelgeuse Workshop 2012, ed. P. Kervella, T. Le Bertre, & G. Perrin, Vol. 60 (Les Ulis: EDP Sciences), 175
Clark, J. S., Ritchie, B. W., & Negueruela, I. 2013, A&A, 560, A11
Crowther, P., & Smartt, S. 2007, A&G, 48, 1.35
Draine, B. T., & Li, A. 2007, ApJ, 657, 810
Dwek, E. 1985, ApJ, 297, 719
Dwek, E. 2006, Sci, 313, 178
Dwek, E., & Arendt, R. G. 2015, ApJ, 810, 75
Dwek, E., Sarangi, A., & Arendt, R. G. 2019, ApJL, 871, L33
Dwek, E., Sarangi, A., Arendt, R. G., et al. 2021, ApJ, 917, 84
Filippenko, A. V. 1982, PASP, 94, 715
Filippenko, A. V., & Foley, R. J. 2005, IAUC, 8484, 2
Fox, O. D., Chevalier, R. A., Dwek, E., et al. 2010, ApJ, 725, 1768
Fox, O. D., Chevalier, R. A., Skrutskie, M. F., et al. 2011, ApJ, 741, 7
Fransson, C., Ergon, M., Challis, P. J., et al. 2014, ApJ, 797, 118
Gall, C., Hjorth, J., & Andersen, A. C. 2011, A&ARv, 19, 43
Gall, C., Hjorth, J., Watson, D., et al. 2014, Natur, 511, 326
Gutiérrez, C. P., Anderson, J. P., Hamuy, M., et al. 2017, ApJ, 850, 89
Hamuy, M., Folatelli, G., Morrell, N. I., et al. 2006, PASP, 118, 2
Inoue, A. K., Hashimoto, T., Chihara, H., & Koike, C. 2020, MNRAS, 495, 1577
Jacobs, B. A., Rizzi, L., Tully, R. B., et al. 2009, AJ, 138, 332
Jacques, C., & Pimentel, E. 2005, IAUC, 8482, 1
Jones, O. C., Kavanagh, P. J., Barlow, M. J., et al. 2023, ApJ, 958, 95
Kotak, R. 2008, in IAU Symp. 250, Massive Stars as Cosmic Engines, ed. F. Bresolin, P. A. Crowther, & J. Puls (Cambridge: Cambridge Univ. Press), 437
Kotak, R., Meikle, P., Pozzo, M., et al. 2006, ApJL, 651, L117
Lebouteiller, V., Barry, D. J., Spoon, H. W. W., et al. 2011, ApJS, 196, 8
Lebouteiller, V., Sloan, G. C., Groenewegen, M. A. T., et al. 2012, A&A, 546, A94
Lucy, L. B., Danziger, I. J., Gouiffes, C., & Bouchet, P. 1989, in IAU Coll. 120: Structure and Dynamics of the Interstellar Medium, ed. G. Tenorio-Tagle, M. Moles, & J. Melnick (Berlin: Springer), 164
Makovoz, D., & Khan, I. 2005, in ASP Conf. Ser. 347, Astronomical Data Analysis Software and Systems XIV, ed. P. Shopbell, M. Britton, & R. Ebert (San Francisco, CA: ASP), 81
Martinez, L., Bersten, M. C., Anderson, J. P., et al. 2020, A&A, 642, A143
Martinez, L., Bersten, M. C., Anderson, J. P., et al. 2022a, A&A, 660, A41
Martinez, L., Bersten, M. C., Anderson, J. P., et al. 2022b, A&A, 660, A40
Matsuura, M. 2017, Dust and Molecular Formation in Supernovae (Berlin: Springer), 2125
Matsuura, M., Dwek, E., Barlow, M. J., et al. 2015, ApJ, 800, 50
Matsuura, M., Dwek, E., Meixner, M., et al. 2011, Sci, 333, 1258
Meikle, W. P. S., Kotak, R., Farrah, D., et al. 2011, ApJ, 732, 109
Niculescu-Duvaz, M., Barlow, M. J., Bevan, A., Milisavljevic, D., & DeÂ Looze, I. 2021, MNRAS, 504, 2133
Nozawa, T., Yoon, S.-C., Maeda, K., et al. 2014, ApJL, 787, L17
Oke, J. B., Cohen, J. G., Carr, M., et al. 1995, PASP, 107, 375
Pereyra, A., Magalhães, A. M., Rodrigues, C. V., et al. 2006, A&A, 454, 827

Perrin, M. D., Sivaramakrishnan, A., Lajoie, C.-P., et al. 2014, Proc. SPIE, 9143, 91433X
Pierel, J. 2024, Space-Phot: Simple Python-Based Photometry for Space Telescopes v1, Zenodo, doi:10.5281/zenodo.12100100
Priestley, F. D., Bevan, A., Barlow, M. J., & De Looze, I. 2020, MNRAS, 497, 2227
Rauscher, T., Heger, A., Hoffman, R. D., & Woosley, S. E. 2002, ApJ, 576, 323
Rest, A., Pierel, J., Correnti, M., et al. 2023, arminrest/jhat: The JWST HST Alignment Tool (JHAT) v2, Zenodo, doi:10.5281/zenodo.7892935
Sarangi, A. 2022, A&A, 668, A57
Sarangi, A., & Cherchneff, I. 2013, ApJ, 776, 107
Sarangi, A., & Cherchneff, I. 2015, A&A, 575, A95
Sarangi, A., Dwek, E., & Arendt, R. G. 2018a, ApJ, 859, 66
Sarangi, A., Matsuura, M., & Micelotta, E. R. 2018b, SSRv, 214, 63
Shahbandeh, M., Fox, O. D., Temim, T., et al. 2025, ApJ, 985, 262
Shahbandeh, M., Sarangi, A., Temim, T., et al. 2023, MNRAS, 523, 6048
Sluder, A., Milosavljević, M., & Montgomery, M. H. 2018, MNRAS, 480, 5580
Sugerman, B. E. K., Ercolano, B., Barlow, M. J., et al. 2006, Sci, 313, 196
Sukhbold, T., Ertl, T., Woosley, S. E., Brown, J. M., & Janka, H. T. 2016, ApJ, 821, 38
Szalai, T., & Vinkó, J. 2013, A&A, 549, A79
Szalai, T., Zsíros, S., Fox, O. D., Pejcha, O., & Müller, T. 2019, ApJS, 241, 38
Szalai, T., Zsíros, S., Jencson, J., et al. 2025, A&A, 697, A132
Truelove, J. K., & McKee, C. F. 1999, ApJS, 120, 299
Verhoelst, T., van der Zypen, N., Hony, S., et al. 2009, A&A, 498, 127
Weaver, T. A., Zimmerman, G. B., & Woosley, S. E. 1978, ApJ, 225, 1021
Wesson, R., Barlow, M. J., Matsuura, M., & Ercolano, B. 2015, MNRAS, 446, 2089
Wesson, R., & Bevan, A. 2021, ApJ, 923, 148
Wooden, D. H., Rank, D. M., Bregman, J. D., et al. 1993, ApJS, 88, 477
Woosley, S. E., Hartmann, D., & Pinto, P. A. 1989, ApJ, 346, 395
Woosley, S. E., Heger, A., & Weaver, T. A. 2002, RvMP, 74, 1015
Zsíros, S., Szalai, T., De Looze, I., et al. 2024, MNRAS, 529, 155
Zubko, V., Dwek, E., & Arendt, R. G. 2004, ApJS, 152, 211